INTERNATIONAL ATOMIC ENERGY AGENCY
UNITED NATIONS EDUCATIONAL, SCIENTIFIC AND CULTURAL ORGANIZATION

INTERNATIONAL CENTRE FOR THEORETICAL PHYSICS
34100 TRIESTE (ITALY) - P.O.B. 586 - MIRAMARE - STRADA COSTIERA 11 - TELEPHONES: 224281/2/3/4/5/6
CABLE: CENTRATOM - TELEX 460392-1

SMR/100 - 69

WINTER COLLEGE ON LASERS, ATOMIC AND MOLECULAR PHYSICS

(24 January - 25 March 1983)

Pulsed Laser Irradiation of Semiconductors: Thermal Description

E. RIMINI

Istituto di Struttura della Materia
Corso Italia, 57
95129 Catania
Italy

L.D. Laude editor - Martinus Nijhoff Publishers

PULSED LASER IRRADIATION OF SEMICONDUCTORS: THERMAL DESCRIPTION

E.Rimini

Istituto di Struttura della Materia - 57 Corso Italia
I 95129 Catania-Italy

Introduction

The use of pulsed laser or electron beams in the nanosecond duration regime and with energy densities of the order of 1 Joule/cm^2 allows to deposite a large amount of energy in short times into the near surface region[1]. Under suitable conditions the irradiation leads to the melting of the surface to a depth of several thousand angstroms. During solidification liquid phase epitaxial regrowth can occur from the underlying single crystal substrate. The irradiation implies also physical conditions far from thermodynamic equilibrium. High quenching rates $\sim 10^9$K/s, high thermal gradients $\sim 10^8$K/cm and velocity of the liquid-solid interface of several meters per second characterize for instance the thermal behaviour for laser irradiation of semiconductors[2].

A tremendous impetus[3] to this subject come soon after the pioneering work of Russian scientists[4] because they showed that damage in ion implanted semiconductors is removed by pulsed or continuous-wave laser irradiation. The term "laser annealing" was then coined, and it is used to day, conventionally, to indicate the overall effects produced during high power irradiation. In the silicon technology laser annealing has several attractive characteristics: it can heat only the region of interest without influencing the inside structure, the process is very fast: one can melt and solidify surface layers in times as short as nanoseconds.

In addition to the potential relevance in the investigation of new processing technologies for silicon integrated circuits, laser irradiation has offered a powerful method to study crystal growth and the impurity incorporation under conditions far from equilibrium. New phases, metastable solutions, formation of amorphous silicon from the melt are only few of the possible new phenomena under investigation[5].

In these lectures I will describe the effects of laser irradiation on ion implanted semiconductors, mainly silicon, for what concerns the structure change from amorphous to single crystal, or from amorphous to poly layer. The basic process responsible of the structure change is reported schematically in Fig.1. The shown case refers to a single crystal overlaid with an amorphous layer and irradiated with a laser or with an electron beam pulse of short duration. The light (or the electron) energy is absorbed by the sample and converted into heat. For a suitable energy density the near surface region can melt. If all the initial amorphous layer is liquid then the subsequent solidification occurs on a single crystal substrate and a liquid phase epitaxy will result. If the thickness of the maximum molten layer is lower than that of the amorphous layer a polylayer will be produced. The previous considerations are valid below a characteristic value of the solid-liquid interface velocity during solidification.

The transient liquid formation is based on the assumption of an "instantaneous" ($\leq 10^{-11}$s) conversion of the photon energy into heat which then propagates inside the sample following the heat equation[6]. A quantitative thermal description of the process requires to account for the changes of optical and

thermal parameters with temperature and structure of the irradiated material, for the absorption and release of latent heat during melting and solidification. The heat diffusion equation should be then solved numerically by computer[7].

As a result of calculations one obtains the melt front penetration, the temperature distribution inside the sample and its time evolution, the velocity of the liquid solid-interface during melting or solidification. These considerations will be detailed in the second part of the paper.

The last section will be devoted to the impurity behaviour[8-9]. After irradiation there is usually a considerable redistribution of impurities introduced for instance by ion implantation. The shape of the final profile depends not only on the dopant species but also on the dynamics of the melting and solidification. One of the most striking manifestation of the rapidly moving liquid-solid interface is the incorporation, or trapping of dopants in the solid at concentrations in excess of the equilibrium solubilities. The interfacial segregation coefficient becomes a unique function of the regrowth velocity. There are several phenomena as constitutional supercooling and cell structure formation which also play a relevant role under these extreme conditions.

Laser irradiation has also stimulated a series of elegant "in situ" measurements to establish the validity of the thermal description over the non thermal hypothesis[10]. These include time-dependent reflection[11-12] and transmission[13] during and following an excitation pulse. The abruptely increase in reflectivity and the drop in transmittivity agree with the optical response of molten silicon, being metallic in character. Other measurements as time dependent Raman scattering[14], time of

flight of evaporated surface atoms[15], time-dependent X-ray Bragg scattering[16] and thermionic-electron emission[17], provide information on different mechanisms: a particular phonon mode, the surface temperature, the strain distribution, the electron kinetic energy and the lattice vibration respectively. Their relationship with the thermodynamic meaning of temperature has been discussed during several round tables at the school. We mention only the fact that in many of these "in situ" measurements a large number of shots is required. In the Raman and X-ray diffraction experiments several thousand of laser pulses are required to obtain a significant number of counts. It is then necessary for instance to guarantee against fluctuation in the energy density, beam uniformity etc, which is not at all a simple matter for lasers.

Measurements of the time dependent electrical resistivity[18] on the other hand provide several useful informations as the melt front extension, the velocity of the solid-liquid interface both during melting and solidification. All these data are obtained in a single pulse and for their relevance in the laser-melting description we will report laser some results.

Crystallization of irradiated layers

Ion implantation offers a reproducible and clean method to produce amorphous layers few thousand angstroms thick. As a starting point we consider the amorphous to single crystal transition and its threshold dependence on the energy density value[19]. This is illustrated in Fig.2a and b for pulsed electron beam and ruby laser irradiation, respectively. In both samples the amorphous layer created by ion implantation

was 1900 Å thick. The sample structure is analyzed by MeV He^+ backscattering in combination with channeling effect techniques. Details of the methods were presented by P.Baeri at the school and are reported in this volume[20].

The aligned yield recorded after irradiation with a 0.55J/cm² energy density of the electron beam decreases drastically and at 0.7 J/cm² coincides with that of unimplanted Si single crystals. The amorphous layer has become single crystal with the same orientation as the substrate. Similar results are found for ruby laser irradiation. Up to 0.9 J/cm² the aligned yield does not change. It decreases at 1.0 and at 1.2 J/cm² it reaches the unimplanted level. The high yield at 0.55 J/cm² for the electron beam and at 1.0 J/cm⁵ for the ruby laser is caused by residual disorder located mainly at the original crystal-amorphous interface. The transition to single crystal occurs at a well defined energy density value and involves the entire disordered layer. Thicker amorphous layers require higher energy densities to become single crystals.

Changes in the structure of the irradiated layer can also be analyzed by diffraction for both transmission and reflection of high-energy electrons. As an example the patterns obtained by the reflection of electrons (RHEED) are shown in[21] Fig.3. The electrons impinge at a glazing angle of few degrees from the surface, and they probe the first few hundred angstroms of the sample. The pattern of the as-implanted Si layer is a diffuse halo characteristic of the amorphous structure. Rings (b) appear in the pattern after ruby laser irradiation and with increasing energy density they change into spots (c).

Rings and spots indicate the presence of a polycrystalline and of a single crystal layer respectively. The poly layer is produced when the thickness of the melted layer does not penetrate all the damaged layer. Solidification occurs before the liquid wets the single-crystal substrate. This statement is clearly demonstrated by the transmission electron microscopy of a cross section of a Si-sample with an initial amorphous layer 1900 Å thick[22]. After irradiation with 0.2 J/cm² ruby laser pulse a polylayer extends from the surface to a depth of about 1000 Å, a residual thin amorphous layer is still present. At the end of the amorphous layer is present a region of damage due to the ion implantation process performed in this case at room temperature. The final aspect is skected in Fig.4b.

Extended defects in the crystallized layers remain for energy density values just above the threshold for the amorphous-to-single crystal transition[23]. In <100> oriented substrate dislocation pairs, v-shaped, are distributed throughout the regrown layer. The dislocations are all of the same length and originate from a thin layer located just behind the initial amorphous region. This is illustrated in the two TEM reported in Fig.5 for a 1000 Å and a 4500 Å thick Si amorphous layer on <100> Si substrate after laser irradiation with a 1.5 and 2.5 J/cm² ruby laser 50ns duration[23], respectively. In the thinner annealed layer the residual defects are small dislocation loops about 1200 Å below the surface, in the thicker annealed layer the defect structure is similar, but the small loops are now located at about

4500 Å below the surface. The length of the V-shaped dislocations increases with the thickness of the amorphous layer, and they originate from the small loops.

It is then the nature of preexisting defects in the transition region between the amorphous and the single crystal substrate free of defects, to determine the amount of residual disorder at the threshold value. In the case of <111> oriented substrate stacking faults are the main type of extended defects at the threshold. They originate also at the preexisting defects at the interface amorphous-single crystal. It has been shown[24], for instance, that a reduction of black spots by thermal anneal at 400°C for ½ hr decreases also the density of stacking faults. At this temperature no regrowth of the amorphous layer occurs by solid phase epitaxy.

The melt front penetration has been investigated[25] by dissolution of precipitates. High temperature diffusion of boron or phosphorus into silicon leads to the formation of precipitates and small loops. After Q-switched irradiation annealed defect-free-regions containing no phosporus precipitates are found in layer of thickness increasing with the pulse energy density as shown in Fig.6a and b respectively. Precipitates originate because the dopant concentration exceeds the solid solubility limit. They dissolve under conditions where impurity diffusion coefficients are extremely high as in liquids. ($\sim 10^{-4} cm^2/sec$) and for elevated quenching rates.

The fast deposition of energy associated to laser irradiation implies also a different description, or at least a more detailed one, of the amorphous recrystallization. The free-energy of the amorphous Si is higher than that of crystalline Si.

Solid phase crystallization occurs because amorphous Si is thermodynamically less stable than crystalline Si. Crystal growth does not occur at room temperature because of kinetic barriers to atom motion. Figure 7 shows schematically the Gibbs free-energy diagram of amorphous, crystalline and liquid silicon[26]. The intersection of the free-energy curves of crystalline and liquid silicon is by definition the equilibrium melting temperature T_c. By a similar extension of the amorphous free-energy curve one obtains the melting temperature T_α, which is lower than that of the crystalline phase. This argument is based on the plausible assumption that the phase transition from the tetrahedral four-fold coordinated amorphous phase to the close-packed 11-12 fold coordinated metallic liquid is first order in nature[27].

The usual heating procedure does not allow the observation of the melting point depression because the amorphous silicon will crystallize in the solid phase before such high temperatures are reached. Only by pulsed irradiation one can hope to avoid crystallization. Heat of crystallization of amorphous Si obtained by ion implantation was obtained recently by differential scanning calorimeter measurements[28]. The obtained ΔH_{ac} value was of 11.3±0.8 and the estimated T_α is depressed of about 250K beneath T_c.

Pulsed electron heating experiments[29] gave some evidence for a substantial reduction in melting temperature of the amorphous material. So far experiments with laser irradiation have been unable to evidence such a depression.

The laser energy is absorbed exponentially with a coefficient depending on the light wavelength and on the target struc-

ture. Large thermal gradients are created during the heating so that usually the region at the interface with the substrate is just above T_α while the liquid at the surface is at a temperature above T_m. Undercooling effects are practically negligible.

Electron beam irradiation creates instead small temperature gradient and by a suitable value of the pulse energy density all the amorphous layer can be undercooled. Temperature distributions similar to these ones can be obtained by laser irradiation on the back side of the sample. The maximum of energy deposition occurs in the amorphous layer at the interface with the single crystal substrate. Heat sink is located on the same side of the heat source and the surface represents a barrier to the heat diffusion. No temperature gradient is practically present in the molten layer.

The upper left side of Fig.8 reports[30] the calculated maximum temperature distributions during the heating for a 30ns Nd laser pulse on a 1500 Å thick amorphous Si layer. For energy density in the 0.9-1.4 J/cm² range the amorphous layer is molten at a temperature below the T_m melting point. In the upper right upper side of the same figure the channeling analysis is shown. Up to 0.7 J/cm² the yield coincides with that of the as-implanted sample. With increasing the energy density of the laser pulse a noticeable decrease of the aligned yield occurs in the energy part corresponding to the region at the interface with the single crystal substrate. About ½ of the amorphous layer is regrown epitaxially with the underlying substrate, the other ½ is a poly layer as found by RHEED.

A double layered structure is formed for temperature of the molten layer below

T_m, similar to the structure found after e-beam irradiation[29]. The experimental data agree closely with calculations using T_α=1200K and $\Delta H_{\alpha-\ell}$=1250 J gr^{-1} for α Si and T_m=1700K and $\Delta H_{c-\ell}$=1780 J gr^{-1} for crystalline Si. The previous measurements with fifferential calorimetry give instead a difference of 400 J gr^{-1} instead of 530 J gr^{-1} as adopted in the calculations[30].

The structure of an ion implanted semiconductor after front (a) or back laser (b) irradiation is reported schematically in Fig.9. For front laser irradiation the sample surface reaches T_α at an energy density E_1. With increasing the energy density the melt front at T_α penetrates inside and all the amorphous layer is molten at E_2. It becomes poly after solidification. In the energy range E_2-E_3 the absorbed energy increases the liquid temperature. Normal liquid at $T>T_m$ near the surface and undercooled liquid at $T<T_m$ near the interface coexist.

The E_2 value represents the energy density threshold for the amorphous-to-single crystal transition but the crystalline quality of the regrow layer is very poor. At energy values higher than E_3 all the initial amorphous layer is above T_m with part of the underlying single crystal substrate molten.

In back laser or electron beam irradiation the amorphous layer starts to melt at an energy density value E_2'. All the layer becomes liquid simultaneously for the low thermal gradient. Up to E_2' value the underlying single crystal is still solid. In the E_1'-E_2' range the molten layer is undercooled, nucleation and fast crystallization occur easily. Above E_2' a good crystalline epitaxial results.

According to the diagram of Fig.7 one can start from a single crystal to obtain a liquid, if it is considerable undercooled during solidification an amorphous structure can result.

This condition is fulfilled when the interface moves at such high velocities that the liquid must be undercooled beneath T_m. Amorphization of crystalline Si has been obtained by ruby laser irradiation with 25 ns pulse duration[31]. Few hundredth thick amorphous layers were obtained for both <111> and <100> substrates. The critical parameter was the velocity of the solid-liquid interface[32].

Thermal description of laser irradiation

Basic process of laser irradiation involves heat generation by the absorption of light and cooling by heat conductivity into the substrate. It has been clearly stated during this school that at least for nanosecond pulse duration the basic assumption of an instantaneous conversion of the absorbed light into heat is justified. Heating and cooling stages are then determined by numerical solutions of the heat equation including a source term due to the absorption of light at a certain depth, the changes of optical and thermal parameters with temperature and structure of the irradiated layer and the latent heat absorbed or generated during phase transitions.

For simplicity we assume a light beam travelling along the z axis normal to the specimen surface, which is uniform in the x-y plane. The target composition is homogeneous in this plane and structural changes occur only in the z direction. Edge effects are also neglected, i.e. the cross section of the laser beam is assumed to be much greater than the heated sample thickness. The heat equation becomes

$$\frac{\partial T}{\partial t} = \frac{\alpha}{\rho C_p} I(z,t) + \frac{1\partial}{\rho C_p \partial z}\left(K \frac{\partial T}{\partial z}\right) \qquad (1)$$

where $I(z,t)$ is the power density of the laser light at depth z and time t. T is the temperature, ρ, C_p, K and α the density, specific heat, thermal conductivity and absorption coefficient of the sample. In a homogeneous medium

$$I(z,t) = I_o(t)(1-R)\ (\exp-\alpha z) \qquad (2)$$

being $I_o(t)$ the temporal power output from the laser and R the target reflectivity. Before considering in detail the solution of eq.(1) it is interesting[6] to illustrate some simple consequences for a rectangular laser pulse of duration τ_p and for constant values of ρ, α, C_p and K.

The heating process involves two characteristic lengths, the absorption α^{-1} and the heat diffusion length $\sqrt{2D\tau_p}$, being $D = \frac{K}{\rho C_p}$ the thermal diffusivity. If $\alpha^{-1} < (2D\tau_p)^{\frac{1}{2}}$ the heat source becomes a surface source (Fig.10a) and the temperature rise is given by[33]

$$\Delta T(z,t) = \left[2I_o(Dt)^{\frac{1}{2}}/K\right] \text{ierfc}\left[z/2(Dt)^{\frac{1}{2}}\right] (1-R) \qquad (3a)$$

for $t<\tau_p$, at the surface z=0 one obtains

$$\Delta T(0,t) = (2I_o/K)\ (Dt/\pi)^{\frac{1}{2}}\ (1-R) \qquad (3b)$$

Approximately the heat required by a layer of thickness $\sqrt{2D\tau_p}$ to increase its temperature of ΔT should be equal to the absorbed energy, i.e.

$$\Delta T \rho C_p (2D\tau_p)^{\frac{1}{2}} \simeq I_o(1-R)\tau_p \Rightarrow \Delta T = \frac{I_o(1-R)}{R} \left(\frac{D\tau_p}{2}\right)^{\frac{1}{2}}. \qquad (4)$$

The energy density to reach a given temperature, as for instance the melting point T_m, is then given by $E_t = \frac{(T_m - T_o)}{(1-R)} \left(\frac{\pi}{4} K\rho C_p\right)^{\frac{1}{2}} (\tau_p)^{\frac{1}{2}}$

The threshold energy density is proportional to $(\tau_p)^{\frac{1}{2}}$, and is independent of the absorption coefficient. Heating and cooling rate are both characterized by τ_p. The heating rate is given by

$$\frac{\Delta T}{\tau_p} = \frac{(I-R)I_o}{\rho C_p (2D\tau_p)^{\frac{1}{2}}} \qquad (5)$$

For instance for $\Delta T = 10^3$K and $\tau_p = 10$ns, the heating rate amounts to 10^{11}K/s. In the case of Silicon the previous consideration requires an absorption coefficient larger $10^5 cm^{-1}$, i.e. a wavelength of about 0.6μm or lower. Thermal diffusivity ranges in between 0.1 and 10 cm^2/sec.

The other extreme case, $\alpha^{-1} >> (2D\tau_p)^{\frac{1}{2}}$, typical of Nd: 1.06 μm wavelength in Si single crystal, implies the non relevance of the heat diffusion and the temperature rise is given by

$$\Delta T(z,t) = (1-R)I_o \alpha \exp(-\alpha z)\, t/\rho C_p \qquad \text{at } t \leq \tau_p. \qquad (6a)$$

at the surface, z=0, and at the end of the pulse, $t=\tau_p$,

$$\Delta T(0,\tau_p) = (1-R)I_o \alpha \tau_p / \rho C_p \qquad (6b)$$

The heating rate, given by $\Delta T(z)/\tau_p$ is then independent of the pulse duration and decreases exponentially with depth. The cooling rate can be estimated assuming that heat diffusion occur over a diatance α^{-1}, then a time $\frac{\alpha^{-2}}{2D}$ is required so that

$$\left.\frac{\Delta T}{\Delta t}\right|_{cooling} = \frac{(I-R)I_o \alpha^3 \tau_p 2D}{\rho C_p} \qquad (7)$$

of the order of 10^8-10^9 K/s.

A detailed treatment requires the numerical solution of the heat equation (1). To this aim the layer of interest is divided in several slices of thickness Δz, and for each of them we should know the following quantities:

1) Temperature of the i-th layer, T_{bi}

2) Structure of the i-th layer: crystalline (0), amorphous (1), liquid (2)

3) Fraction of the i-th layer which is melted FF_i

4) Thermal and optical parameters for each layer, function of $(T_{bi}, \{0,1,2\}, FF_i)$.

Let us compute the temperature change with time in the i-th slice. The power density incident is given by $I_i = I_{i-1} e^{-\alpha_{i-1}\Delta z}$ $(I_1 = I_o(t)(I-R))$, and the energy absorbed during Δt is

$$\Delta Q_{abs} = I_i (1 - e^{-\alpha_i \Delta z})\Delta t, \qquad (8a)$$

the energy exchanged by thermal diffusion with the slice i-1 and i+1 is given by

$$\Delta Q_{diff} = \left| K_- \frac{T_{bi-1} - T_{bi}}{\Delta z} + K_+ \frac{T_{bi+1} - T_{bi}}{\Delta z} \right|$$

with $K_- = (K_{i-1} + K_i)/2$, $K_+ = (K_{i+1} + K_i)/2$. $\qquad (8b)$

The temperature rise is then given by

$$T_{bi}(t+\Delta t) = T_{bi}(t) + \frac{\Delta Q_{abs}+\Delta Q_{diff}}{\rho C_p \Delta z} \qquad (9)$$

If $T_{bi}(t)<T_m\leq T_{bi}(t+\Delta t)$ melting should be considered, if instead

$T_{bi}(t)>T_m\geq T_{bi}(t+\Delta t)$ solidification has occurred. In both cases the latent heat should be included. The energy av ilable for melting if $T_{bi}(t)\leq T_m$ or released from solidification if $T_{bi}(t)>T_m$ is obtained by

$$\Delta Q_i' = \Delta Q_{abs}+\Delta Q_{diff}-(T_m-T_{bi})\rho C_p \Delta z$$

This energy determines the variation in the fraction of the molten layer, FF_i infact

$$\Delta FF_i = \frac{\Delta Q_i'}{\rho \Delta z \Delta H_m}$$

with ΔH_m enthalpy of melting or solidification. The new value for FF_i at time, $t+\Delta t$, is

$$FF_i(t+\Delta t) = FF_i(t)+\Delta FF_i \qquad (12)$$

The new fraction can be lower, equal or larger than 1. If $0\leq FF_i\leq 1$ the temperature $T_{bi}(t+\Delta t)$ is maintained at T_m; if $FF_i>1$, the surplus of absorbed energy $\Delta Q_i'' = (FF_i-1)\rho\Delta z\Delta H_m$ is used to rise the temperature of the slice above T_m, i.e. $T_{bi}(t+\Delta t)=T_m+\Delta Q_i''/\rho C_p \Delta z$. Then the calculation proceeds to the next slice and so on. The numerical approach requires as stability condition the following disequality $K\Delta t/\rho C_p(\Delta z)^2<\frac{1}{2}$ between Δt and Δz, time interval and space interval respectively.

In addition one uses as boundary conditions, the temperare distribution in the target at t=0, no loss of heat occurs at any time from the irradiated surface, and for a bulk sample $\lim_{z\to\infty} T$ is constant at any time t.

As an illustration of the method we report the following examples which refer to ruby laser irradiation of Si single crystal. The pulse duration is 30 ns, i.e. a gaussian shape is assumed with a FWHM of 30ns. The time dependence of temperature at three different depths inside the crystal is shown in Fig.11 for 1.2 J/cm² energy density pulse. The surface layer reaches the melting temperature just after 30 ns from the switch-on of the laser pulse, then the temperature remains constant because the absorbed energy is used as latent heat for melting. The temperature increases later and reaches a maximum value of 2×10^3K at the end of the pulse. The layer at a distance of 90 nm from the surface reaches the melting point at a later time and so on. Cooling occurs with a rate of 10^9K/sec for all the considered layers, while the heating rate if of the order of 10^{11}K/s.

Melt front penetration and its dependence on the energy density are shown in Fig.12. Threshold for melting just the surface layer corresponds to 0.8 J/cm². With increasing the energy density increases also the thickness of the molten layer and the time interval during which the surface is liquid. In Si irradiated with ruby laser a typical rate of 0.6 μm /J/cm² is obtained. The melting proceeds with a planar front at a velocity of about 10 m/s, solidification usually occurs in a time interval of about then times the pulse duration.

During solidification the heat of melting liberated at the advancing solid-liquid interface has to be transported by heat conduction into the substrate, i.e.

$$\Delta H_m \rho \cdot v = K_s \left.\frac{\partial T}{\partial z}\right|_s - K_\ell \left.\frac{\partial T}{\partial z}\right|_\ell \qquad (13)$$

where v is the velocity of the liquid-solid interface and the subscripts s and ℓ refer respectively to the solid and liquid phases. The equation does not include undercooling effects at the interface. Usually the temperature gradient in the liquid is much smaller than that in the solid so that the velocity is determined mainly by the temperature gradient in the solid. For instance if the energy density is just enough to melt the layer initially at room temperature and if $\alpha^{-1} << \sqrt{2D\tau_p}$, one can estimate

$$\frac{\partial T}{\partial z} = \frac{T_m - 300}{\sqrt{2D\tau_p}}; \quad \text{for Si } (D=0.1 \text{ cm}^2/\text{s}) \quad v = \frac{1\times10^{-3}}{\sqrt{\tau_p}} \text{ (m/sec)}. \quad (14)$$

With increasing the energy density also the melt duration increases too and solidification starts after the end of the laser pulse. The time interval τ_p becomes then the melt duration t_m which is proportionally to the square of the energy density, E^2. The velocity becomes inversely proportional to the energy density value. In the other case of $\alpha^{-1} > \sqrt{2D\tau_p}$, the regrowth is independent of the pulse duration, and it is given by $T_m\ \alpha/e$. The maximum velocity is reached in any case near the energy threshold value. Short pulses reduces in addition considerable the heat diffusion length.

This analysis is based on a simple description of the process, and it is necessary to support it by experiments. With this aim measurements[18] of the electrical conductance of Si during the irradiation process were undertaken. They yield direct measurements of important dynamic parameters as the melt depth, the front velocity and the solidification. In these experiments one takes advantage of the large increase (≈30 times) of conductance of Si upon melting. Samples are irradiated with ruby laser pulse and for each pulse the electrical conductivity is measured as a function

of time. Particular care must be paid to reduce substantially the photoconductive response, so that the entire melt conductance is not masked by it. Si samples doped with Au, to decrease the carrier lifetime, were used.

Simultaneous measurements of the surface reflectivity by a Ne-He laser were used to confirm that melting had occurred, to determine the time during the laser pulse at which the melt started, and to measure the melt duration[34]. A typical set of measurements is shown in Fig.13. The time dependent voltage V(t) is reported for a variety of incident laser energy densities in the lower part of the figure. The signal observed for energy densities below the melt threshold, 0.8 J/cm^2, is due to the photoconductivity in Si. Above the threshold value the transient voltage curves show the conductance increasing in magnitude and duration after the photoresponse.

The reflectance signal reported in the upper part of the same Fig.13 indicates the onset of the high reflectivity phase, and its duration. It is clear that at 0.57 J/cm^2 no melting of the surface has occured, and that at 0.2 J/cm^2 the surface remains liquid for a larger time than at 1.65 J/cm^2 irradiation.

Comparison of experimental data with calculation is reported in Fig.14. The voltage dependence data shown in Fig.13 are converted into melt depth through a detailed analysis in which the other contributions to the conductance in addition to that of molten Si alone are estimated. The good agreement between the experimental results and the calculations support the thermal description. The slopes of the curves in Fig.14

provide the velocity of the liquid-solid interface during cooling. Also these values of few meters per second, are in agreement with the predictions of the thermal model.

Dopant incorporation

The formation of a liquid layer modifies the profiles of the implanted impurities. Diffusion in molten Si occurs with a coefficient of 10^{-4}cm^2/sec and detactable migration takes place during the time interval, ∿100ns, the near surface region remains liquid. Impurities after irradiation are then electrically active and redistribute in depth[35]. The sheet resistance of Si samples implanted with 40 keV -10^{16} As/cm^2 is reported in Fig.15 as a function of the energy density for Nd/YAG double frequency pulse. At an energy density of about 0.4 J/cm^2 the abrupt decrease of the sheet resistance(•) is related to the melting of the surface region. Dissolution of As complexes occurs also at the same energy value as shown for the samples irradiated after thermal annealing (o). The As distribution is shown in Fig.16 before and after irradiation with 0.6 J/cm^2 energy density pulse.

Profile broadening is not the only observed effect. Several impurities show in addition a partial surface accumulation as reported in Fig.17 for Sb[36] and Cu[37]. For Sb the profile depends on implantation and irradiation conditions whilst for Cu complete surface accumulation is always observed. The redistribution of the impurities during solidification is governed by the equilibrium distribution coefficient, K_o, defined as $K_o = \left.\frac{c_s}{c_\ell}\right|_{eq}$ where c_s and c_ℓ are the concentrations in the solid and liquid phase determined by the phase diagram at a fixed temperature close to the melting point. If $K_o<1$ impurities are rejected at the interface toward

the liquid where they are allowed to diffuse.

Normal crystal growth occurs at a velocity of the solid-liquid interface of about 10^{-5}m/s, i.e. five orders of magnitude lower than that obtained by laser irradiation. In these conditions K_o is meaningless and the redistribution is determined by the interfacial redistribution coefficient $K' = \left.\frac{c_s}{c_\ell}\right|_i$. Experiments indicate that K' for a large number of impurities should be much larger than K_o, and in addition the dopant concentration retained in substitutional lattice sites can be several order of magnitude larger than the equilibrium solubility[36].

The dynamic of the dopant redistribution is reported in Fig.18 where the profiles both in the liquid and solid phase are shown at different stages of the solidification process. The continuous rejection of impurity at the interface will result in surface accumulation, as the last layer will freeze. These profiles are obtained following a procedure similar to that reported with some details in the previous section on the heat flux calculation.

The process described by the calculations[7] are the following ones:

i) diffusion in the liquid phase of the initial implanted distribution, accounting for the l-s interface kinetics, as determined by heat flow calculations.
ii) impurity rejection from the solid to the liquid phase, according to a K' fitting parameter
iii) diffusion of the impurities rejected by the interface in the liquid.

This simple description combine both mass and heat transport, but no interference between these two processes is considered. From the fit of the experimental data with calculations it has been inferred that K' is velocity dependent[38]. The amount of surface segregation changes with the liquid-solid velocity during solidification. The velocity can be changed in several ways: by changing the pulse duration, or the coupling of the laser beam with the substrate, or the target temperature[39].

Figure 19 reports as an illustration[40] the molten thickness vs time for a ruby (0.69 μm) and Nd (1.06 μm) laser irradiation of Si single crystals and 10^2nm thick amorphous layer on single crystals. The solid-liquid interface velocity given by the slope of molten thickness-time and averaged over the least hundred nm changes from 0.5 to 3.3 m/s. In the presence of impurities the solidification leads to segregation. As an example the depth profiles of Te implanted in Si and irradiated with a Nd laser pulses are shown in Fig.20. The lower part reports the profile after irradiation with 2.0 J/cm^2 for aligned and random incidence of the analyzing 2.0 MeV He^+ beam.

The Te accumulation at the surface amounts to 20% and is easily obtained by the aligned yield. The large attenuation for the in-depth distribution indicates that the majority of the remaining Te atoms are substitutionally located. The calculated solidification velocity is ∿3.0 m/s. Channeling effect in combination with MeV He^+ Rutherford backscattering provides a simple and a reliable method to determine the total amount of rejected impurities at the surface. The profile determination is limited by the depth resolution of the technique which is hardly pushed below the 5 nm.

If the implanted sample is annealed before irradiation the Te profile shows a much larger surface accumulation as shown in the upper part of Fig.20. The small absorption coefficient of the Nd wavelength in Si single crystal produces small temperature gradient and the calculated solidification velocity is about 0.8 m/s. To reduce the required energy density for melting the sample was heated at about 300°C during irradiation. The K' fitting values are 0.5 and 0.03 for the higher and lower velocity respectively. The stimated K_o equilibrium value is ∿10^{-4}.

Similar results are obtained by changing the substrate temperature during irradiation[40]. As an illustration Fig.21 reports Te distribution profiles after irradiation with ruby laser pulse of 30ns duration and 1.5 J/cm^2 energy density at different substrate temperatures. The higher surface accumulation is obtained at 600K substrate temperature. The solid liquid interface velocity changes are associated to the dependence of the thermal conductivity on temperature.

The major result of these experiments is the unique relation between the K' value needed to fit the surface accumulation and the solid-liquid interface velocity independent of the way it was obtained. A typical K'-v trend is shown in Fig.22 for Bi implanted Si samples[38]. The K' value seems to saturate at a value <1. Although measurements at higher velocities would be of interest they are limited by the amorphous formation occurring at solidification velocities of ∿20 m/s. Under these conditions the usual definition of K' loses its significance.

The data of Fig.22 refer to different substrate orientations. At low velocities the (111) oriented Si substrates give rise

to less segregation than the (100) crystal substrates[38]. ge velocities the two values almost coincide. The understanding of the orientation dependence requires a detailed description of the crystal-liquid interface morphology. So far two different possible mechanisms have been considered. The amount of undercooling required to grow a given liquid at a fixed speed is larger for (111) than for (100) substrate orientation. The increased undercooling give rise to an increased amount of trapped impurities[41] The other mechanism [42] is based on the atomistic description of the different faces. The density of ledges in the (111) plane is smaller than that in the (100) plane thus requiring a greater lateral velocity to maintain the same solidification rate. This faster lateral growth will produce larger dopant trapping in the (111) oriented substrates.

The dependence of K' on velocity is related to the kinetic aspects of the segregation process. In a simple view two different times should be considered; the time required for the interface to move one interatomic distance during solidifiaction, $\tau_g = \frac{\lambda}{v}$, with λ interatomic distance, and the residence time, $\tau_r = \frac{\lambda^2}{D_i}$, with D_i diffusion of coefficient of the impurity at the interface. Trapping of the impurity can occur if the dopant resides in the near interface region longer than the time required to regrow it, i.e., if $\tau_g < \tau_r$. In the opposite case the dopant is rejected into the high solubility phase, i.e., into the liquid. The critical velocity above which trapping K' increases steeply is then $v_{crit} = D_i/\lambda$.

The diffusion coefficient D_i is estimated[43] by the relationship

$D_i \simeq \sqrt{D_s D_\ell}$, where the subscripts s and ℓ refer to solid and liquid phases respectively. The interface is assumed to have properties intermediate between those of the two adjacent media. D_ℓ is of the order of $10^{-4}cm^2/s$ for any dopant in Si, while D_s ranges from $10^{-11}cm^2$ for the slow (Bi,As,Sb...) to $10^{-4}cm^2/s$ for the fast (Cu,Ag,Au...) diffusers in Si at temperature close to the melting point.

These D_i estimates give v_{crit} values of the order of few cm/s and of few m/s for slow and fast diffusers in Si respectively. The experimental data so far obtained by laser irradiation agree with these estimates. In the case of fast diffusers the velocity obtained by irradiation is not sufficient to trap them into the lattice[44].

The concentration of dopant trapped in substitutional positions exceeds the solid solubility value of several orders of magnitude. However the maximum solubility obtained by laser irradiation seems to be limited by three mechanisms[45]: interface stability, mechanical stress and thermodynamics limit.

The solid-liquid interface can proceed flat according to the classical work of Mullins and Sekerka[46] if

$$G_\ell > \frac{vm\ c_s(i)}{D_\ell}\ \left(\frac{1-K'}{K'}\right)$$

The term on the left is the temperature gradient in the liquid close to the interface and that on the right is the gradient obtained from the phase diagram and taking into account the dopant concentration in the liquid close to the interface. In the

case the disequality is not fulfilled, interfacial instability develops and cell formation occurs. The instability is caused by constitutional supercooling in the liquid at the interface. By increasing the thermal gradient in the liquid the onset of instability is delayed. This implies that the regrowth velocvity must be increased.

An example of cell formation in laser irradiated In implanted Si samples is shown by the TEM micrographs reported in Fig.23 [47]. The upper part and the lower part refers to a sample in which the regrowth velocity was 3 m/s and 1.5 m/s respectively. The interface breakdown and then the cell size occurs on the scale of D/v. At the high regrowth velocities encountered in laser irradiated semiconductors the cell size ranges between few hundredth and few thousands angstroms.

Constitutional supercooling is the most common limit to supersaturation but other mechanisms can be present. In the case of boron the large difference in covalent radius between the dopant and the Si host results in large uniaxial strain[45]. The limit to the maximum substitutional concentration is due to the limit of elastic properties of Si and extended defects results at high concentrations.

An absolute thermodynamic limit[48] to solute trapping is given at the intersection between the solidus and the liquidus free energy curves. This is a very general limiting conditions and it is not yet clear if it can be reached.

Conclusions

The aim of these lectures was to present the laser irradiation effects in ion implanted semiconductors and to describe them in terms of melting model. Structure changes, residual defects and dopant incorporation are all explained by this simple thermal description. In addition several predictions of the model have been and can be used as a guide for further investigations.

REFERENCES

1) J.M.Poate and G.Foti editors "Surface Modification and Alloying" Nato Advanced Institute Series - Plenum Press, N.Y.,1983

2) P.Baeri,S.U.Campisano,G.Foti, and E.Rimini, J,Appl.Phys.50,788(1978)

3) See for instance the proceedings of the Material Research Society Conferences (Boston Meeting) on this subject.(i) Laser-Solid Interactions and Laser Processing (Edited by S.D.Ferris,H.J.Leamy and J.M.Poate). A.I.P.Conf.Proc.50, New York (1979); (ii) Laser and Electron Beam Processing of Materials (Edited by C.W.White and P.S.Peercy). Academic Press,New York1980); (iii) Laser and Electron-Beam Solid Interaction and Materials Processing (Edited by J.Gibbons, L.D Hess and T.W.Sigmon). North Holland, New York (1981); (iv) Laser and Electron Beam Interaction with Solids (Edited B.R.Appleton and G.K.Celler). North Holland, New York(1982).

4) Khaibullin, I.B.Shtyrkov,E.J.,Zaripov,M.M.,Galyautdinov, M.F.and Zakirov,G.G.,Sov.Phys.Semicond. 11,190(1977); Antonenko,A.Kh.,Gerasimenko,N.N.,Dvurechenskii,A.V.Smirnov, L.S. and Tseiitlin, Sov.Phys.Semicond. 10,81(1976).

5) E.Rimini,Physica Scripta - October (1982) J.M.Poate and W.L.Brown - Physics Today, 35,6-24(1982)

6) N.Bloembergen, in "Laser-Solid Interactions and Laser Processing" (S.D.Ferris, H.J.Leamy, and J.M.Poate eds).p.1 A.I.P. n.50 N.Y.(1979).

7) P.Baeri and S.U.Campisano in "Laser and Electron Beam Processing of Semiconductor Structures" J.W.Mayer and J.M.Poate editors (Academic Press,N.Y.)1982, chap.4

8) C.W.White,D.M.Zehener,S.U.Campisano and A.G.Cullis in "Surface Modification and Alloying" J.M.Poate and G.Foti Editors (Plenum Press, N.Y.) 1983; Chap.4

9) S.U.Campisano "Non equilibrium dopants incorporation in silicon melted by laser pulses" Appl.Phys. (in press).

10) J.A.van Vechten "Plasma annealing and laser sputtering: role of the Frenkel excitons" - this volume

11) D.H.Auston,C.M.Surko,T.N.C.Venkatesan,R.E.Slusher and J.A.Golovchenko; Appl.Phys.Lett. 33,437(1978)

12) D.H.Auston,C.M.Surko,T.N.C.Venkatesan,R.E.Slusher and J.A. Golovchenko; Appl.Phys.Lett.35,635(1979)

13) D.H.Lowndes, Phys.Rev.Lett. 48,267(1982)

14) H.W.Lo and A.Compaan; Phys.Rev.Lett. 44,1604(1980)

15) S.Stritzker, P.Pospieszcyk and J.A.Tagle; Phys.Rev.Lett. 47,356(1981)

16) C.Larson,C.W.White,T.S.Noggle and D.Mills; Phys.Rev.Lett. 48,337(1982)

17) R.Yen,J.M.Liu,H.Hurz and N.Bloenbergen, Appl.Phys. A27, 153(1982)

18) G.J.Galvin,M.O.Thompson, J.W.Mayer,R.M.Hammond,N.Paulter and P.S.Peercy; Phys.Rev.Lett. 48,33(1982)

19) G.Foti and E. Rimini in "Laser and Electron Beam Processing of Semiconductor Structures" J.W.Mayer and J.M.Poate editors (Academic Press, N.Y.(1982)) Chapt.2.

20) P.Baeri-"Rutherford Backscattering: from principles to application in laser annealing"- this volume

21) G.Vitali,M.Bertolotti,G.Foti and E.Rimini, Phys.Lett. A63,351(1977)

22) A.G.Cullis,H.C.Webber,D.V.Mc Caugham,and N.G.Chew - In "Laser and Electron Beam Processing of Materials"(C.W.White and P.S.Peercy eds). p.183- Academic Press N.Y.-1980

23) G.Foti,E.Rimini,W.F.Tseng, and J.W.Mayer,Appl.Phys. 15,365(1978)

24) S.U.Campisano,G.Foti and M.Servidori, Appl.Phys.Lett. 36,279 (1980)

25) J.Narajan, Appl.Phys.Lett. 34,312(1979)

26) F.Spaepen and D.Turnbull in 3(i),p.73

27) B.G.Bagley and H.S.Chen in 3(i),p.97

28) J.M.Poate "Some Thermodynamics Properties of Amorphous Si" IBMM-Grenoble Sept.5-10 1982 (Nucl.Instr.Meth. to be published)

29) P.Baeri,G.Foti,J.M.Poate, and A.G.Cullis Phys.Rev.Lett. 45,2036(1980)

30) P.Baeri,S.U.Campisano,M.G.Grimaldi and E.Rimini, J.Appl. Phys. (Nov.1982)

31) A.G.Cullis, H.C.Webber and N.G.Chew in 3(iv) ,p.131

32) A.G.Cullis,H.C.Webber, N.G.Chew,J.M.Poate and P.Baeri: Phys.Rev.Lett. 49,219(1982)

33) J.F.Ready "Effects of high power laser irradiation" Academic Press,N.Y.1971, Chap.4

34) G.J.Galvin, M.O.Thompson,J.W. Mayer, P.S.Peercy,R.B.Hammond and N.Paulter "Time-Resolved Conductance and Reflectance Measurements of Silicon Solidification from the Melt During Pulsed Laser Annealing" Phys. Rev. to be published.

35) E.Rimini,W.K.Chu and S.R.Mader, J.Appl.Phys. 52,3696(1981)

36) C.W.White, S.R.Wilson,B.R.Appleton and F.W.Young jr. J.Appl.Phys.51,738(1980).

37) P.Baeri,S.U.Campisano,G.Foti and E.Rimini, Phys.Rev.Lett.41,1246(1978)

38) P.Baeri,G.Foti,J.M.Poate,S.U.Campisano and A.G.Cullis, Appl.Phys.Lett. 38,800(1981)

39) A.G.Cullis,H.C.Webber,J.M.Poate and A.L.Simons, Appl.Phys.Lett. 36,320(1980)

40) G.Foti, to be published

41) K.A.Jackson and G.H.Gilmer - to be published

42) D.Turnbull and F.Spaepen Chapter 2 in "Laser Annealing of Semiconductors" eds J.M.Poate and J.M.Mayer, Academic Press N.Y. 1982

43) B.K.Jindall and W.A.Tiller, J.Chem.Phys. 49,4632(1968).

44) M.J.Aziz, J.Appl.Phys. 53,1158(1982)

45) C.W.White in ref.3 (iv) p.109

46) W.W.Mullins and R.F.Sekerka, J.Appl.Phys. 35,444(1964)

47) A.G.Cullis,R.Series,H.C.Webber and N.G.Chew in "Semiconductor Silicon 1981" Electrochemical Society, N.J.1981 -p.518

48) J.C.Baker and J.W.Cahn, Acta Met. 17,575(1969).

Figure Captions

Fig.1 - Schematic of crystallization in amorphous Si on single crystal substrate by electron or Q-switched laser pulse irradiation.

Fig.2 - Analysis with 2.0 MeV and 1.8 MeV He^+ beams in combination with channeling effect of recrystallization of a 1900 Å-thick amorphous Si on a (100) oriented substrate after irradiation with electron beam (a) and with ruby laser (b) pulse of different energy density.

Fig.3 - Reflection high-energy electron diffraction (RHEED) patterns of an as-implanted amorphous layer (a), after 1.25 J/cm^2(b) and 5.0 J/cm^2(c) ruby laser pulses, respectively. The azimuth direction is along the <110>

Fig.4 - Transmission electron micrograph of a cross section of a 1900 Å thick amorphous layer on Si <100> substrate after irradiation with 0.2 J/cm^2 ruby laser 15 ns pulse duration (a); schematic of a back-thinned implanted silicon sample for TEM analysis (b).

Fig.5 - Transmission electron micrograph of 10^3 Å thick (a) and 4.5×10^3 Å thick (b) amorphous implanted Si layers after irradiation with 1.5 and 2.5 J/cm^2 ruby laser pulses respectively. The dislocations originate from small loops and their lenghts scale with the thickness of the initial amorphous layer.

Fig.6 - Bright-field electron micrograph of a phosphorus-diffused silicon specimen shown dissolution of precipitates after ruby laser irradiation. The annealed depth increases with the energy density of the ruby laser single pulse. The thickness of the defect-free regions can be measured from thickness fringes. (a) 2.0 J/cm^2, (b) 3.0 J/cm^2.

Fig.7 - Free-energy diagram of amorphous, crystalline and dense metallic liquid silicon. T_α and T_m are the melting point of the amorphous and of the crystalline phase respectively. In the energy density E_1-E_2 the molten layer is undercooled.

Fig.8 - Back-irradiation of a 1500 Å thick amorphous Si layer with 30ns Nd glass laser pulse irradiation. The computed temperature profiles at several energy densities are shown in the left side. T_α and T_m represent the melting point of amorphous and crystalline Si respectively. Right hand side: experimental RBS spectra for aligned incidence of 2.0 MeV He^+ beam after irradiationat several energy density.

Fig.9 - Melt front penetration for front and back irradiation. The resulting structures are indicated in the lower part.

Fig.10 - Schematic laser pulse intensity and temperature profiles for a penetration depth, α^{-1}, of the light small (a) and large (b) compared to the thermal diffusion length.

Fig.11 - Temperature-time dependence at different depths for Si single crystal irradiated with 30ns ruby laser pulse of 1.2 J/cm^2 energy density.

Fig.12 - Kinetics of melt front in Si single crystals irradiated with 30 ns ruby laser pulses of different energy densities.

Fig.13 - (a) Signal from the reflected He-Ne probe laser as a function of time for three incident laser energy densities Electrical conductance, as measured by the voltage across the scope load resistor, as a function of time.

Fig.14 - Experimental (heavy line) and computer calculated (light line) melt depths as a function of time for several incidence laser energy densities above the melt threshold.

Fig.15 - Sheet resistance of 40 keV-10^{16} As at/cm^2 implanted Si samples vs. energy density of 20 ns pulse duration Nd:YAG double frequency. Full circles refer to as implanted samples, open to thermally annealed samples.

Fig.16 - Broadening of the As-impurity profile after irradiation with a 20ns pulse duration of Nd:YAG double frequency -0.6 J/cm^2.

Fig.17 - Changes in the impurity profiles after laser irradiation.

Fig.18 - Calculated impurity profiles at different times for and initial gaussian concentration distribution. The solidification proceeds from right to the left with a solid-liquid interface velocity of 2m/s and for an interfacial distribution coefficient $K'=0.1$

Fig.19 - Kinetic of the melt thickness for Nd and ruby laser pulse irradiation of Si single crystals and of Si samples with 0.1 μm thick amorphous layer.

Fig.20 - Te depth profiles for Nd laser irradiation of Si single crystals (upper part) and of Si with 0.1 μm thick amorphous layer (lower part). The arrow indicates the position of the projected range for the as-implanted Te distribution. The data refer to random (Δ) and to aligned (▲) incidence of the 2.0 MeV He^+ analyzing beam.

Fig.21 - Te depth profiles after irradiation with 30 ns ruby laser pulse of 1.5 J/cm^2 at different substrate temperatures.

Fig.22 - Bi segregation coefficient (K') in (100) and (111) Si oriented substrates as a function of the liquid-solid interface velocity.

Fig.23 - Transmission electron micrographs showing the cell formation and its dependence on the solid-liquid velocity for In implanted Si samples, ruby laser irradiated.

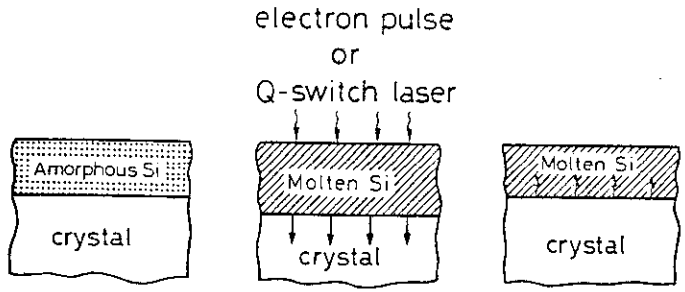

Fig. 1

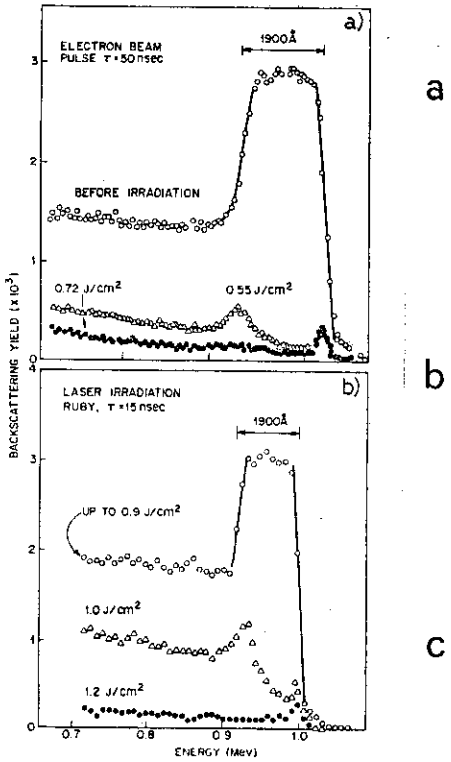

Fig. 2

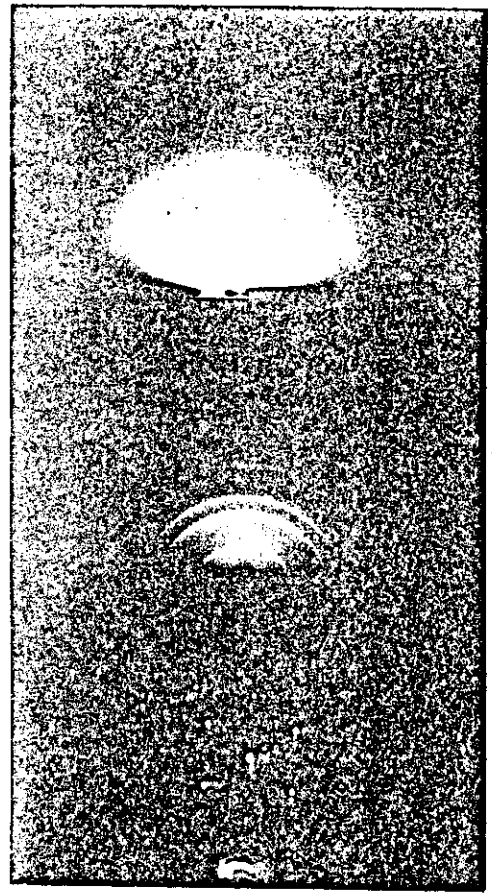

Fig. 3

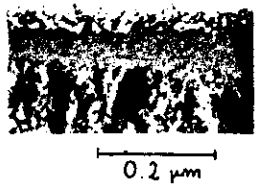

Fig. 4 a

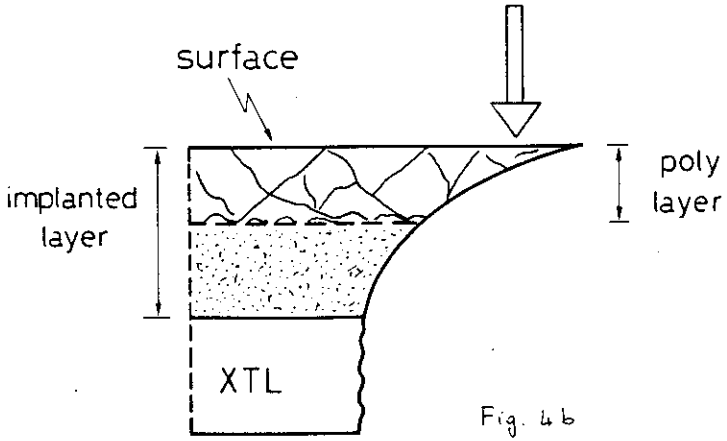

Fig. 4 b

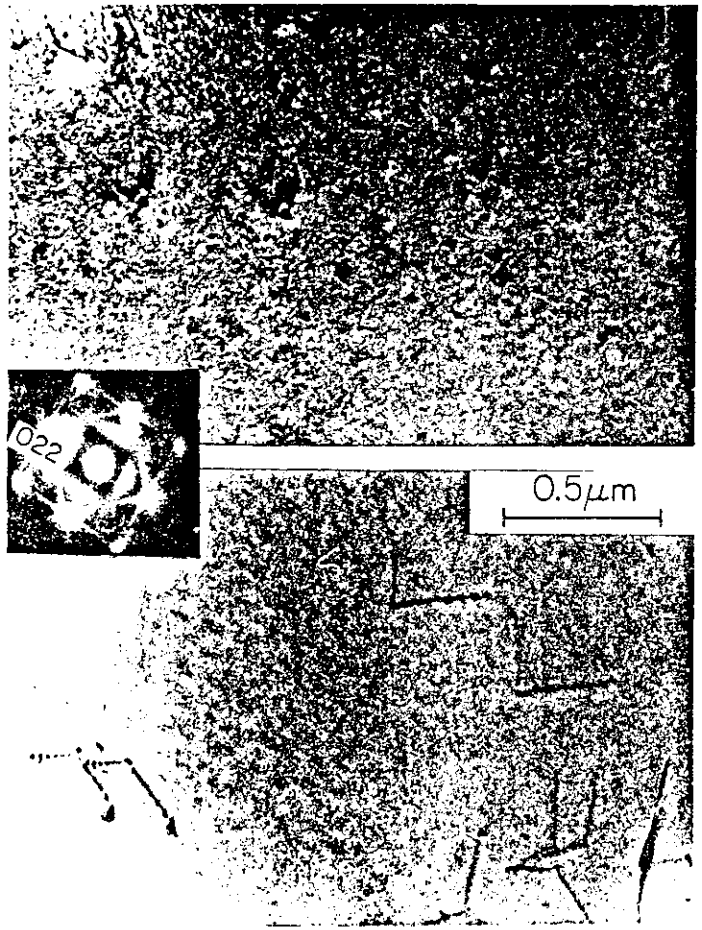

Fig. 5

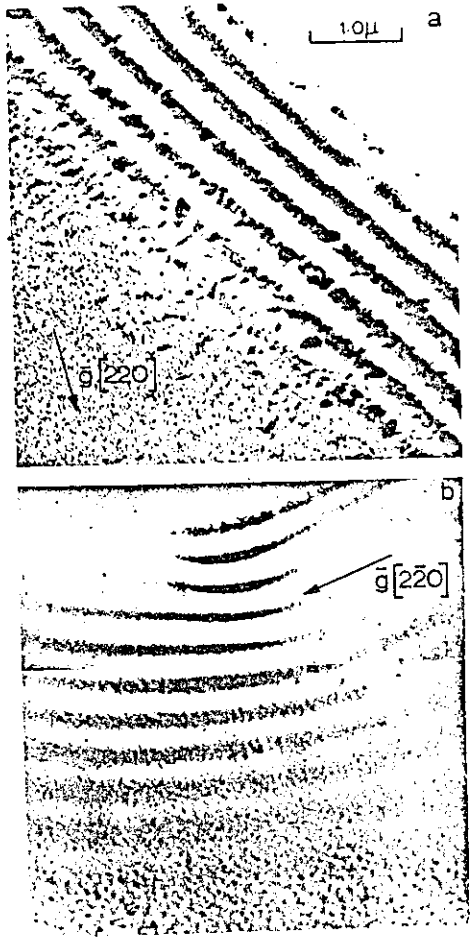

Fig. 6

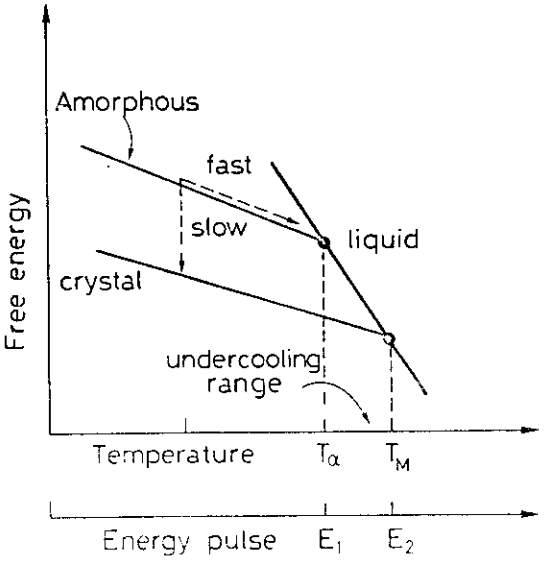

Fig. 7

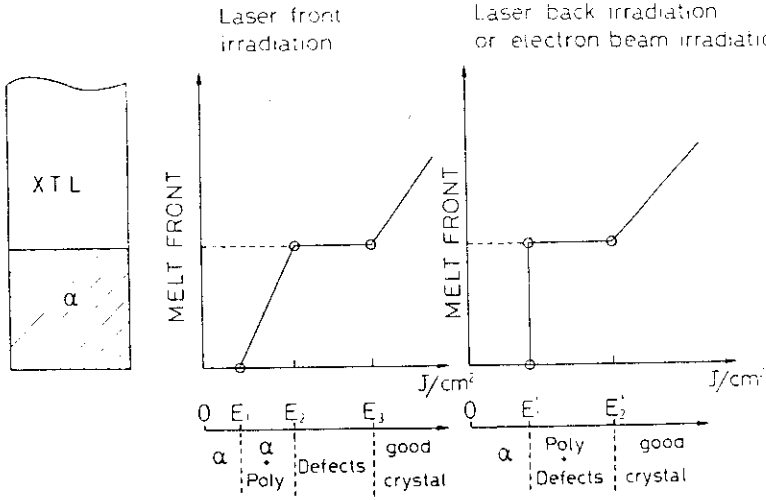

Fig. 8

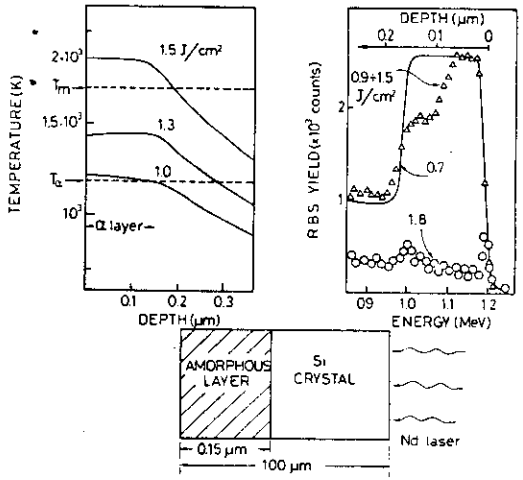

Fig. 9

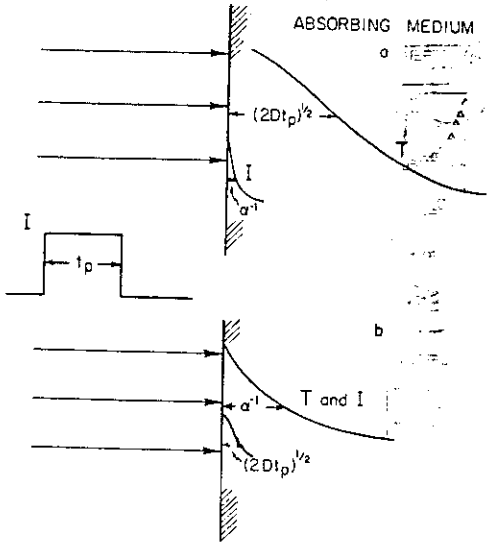

Fig. 10

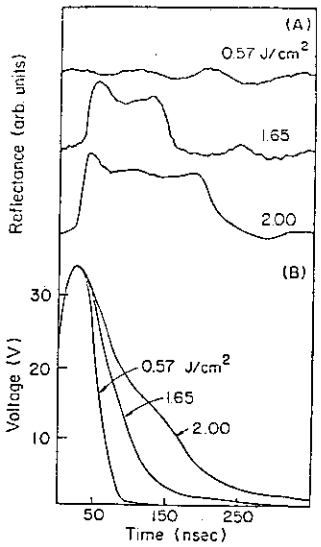

Fig. 13

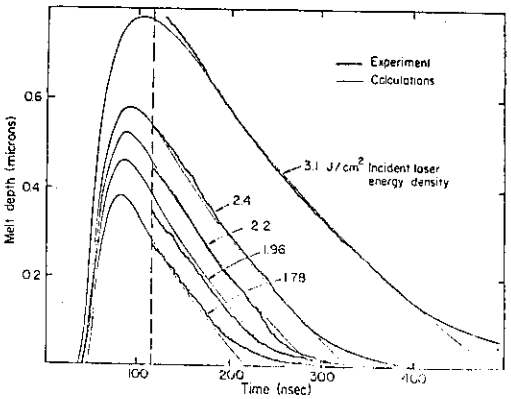

Fig. 14

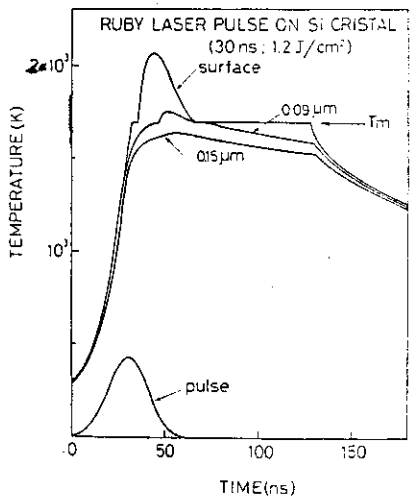

Fig. 11

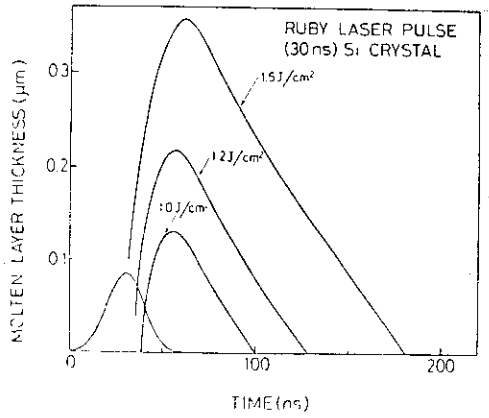

Fig. 12

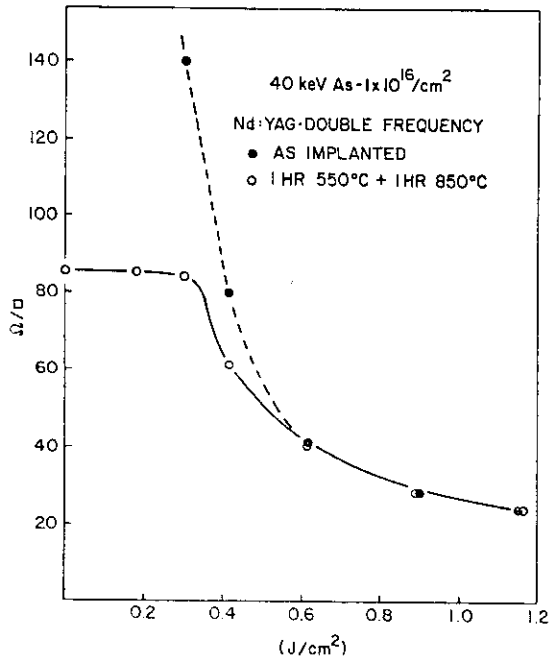

Fig. 15

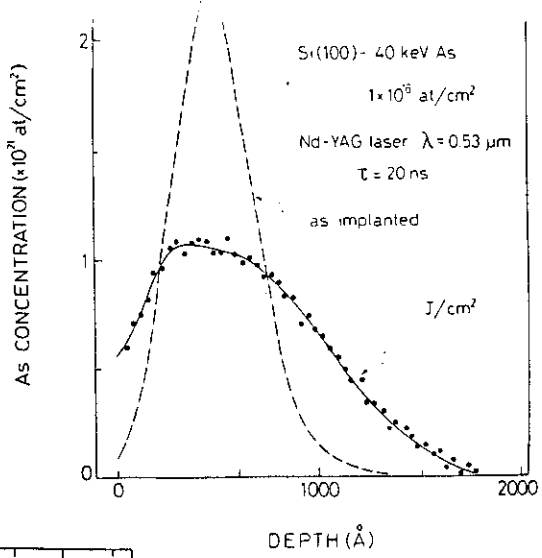

Fig. 16

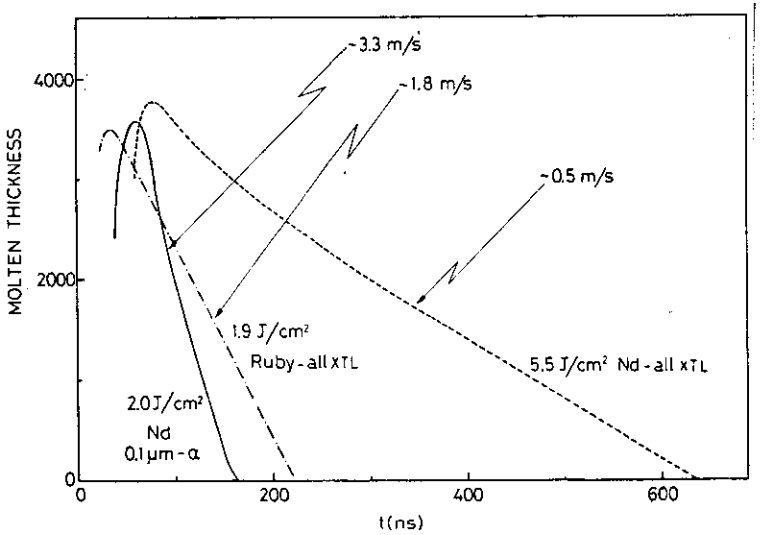

Fig. 19

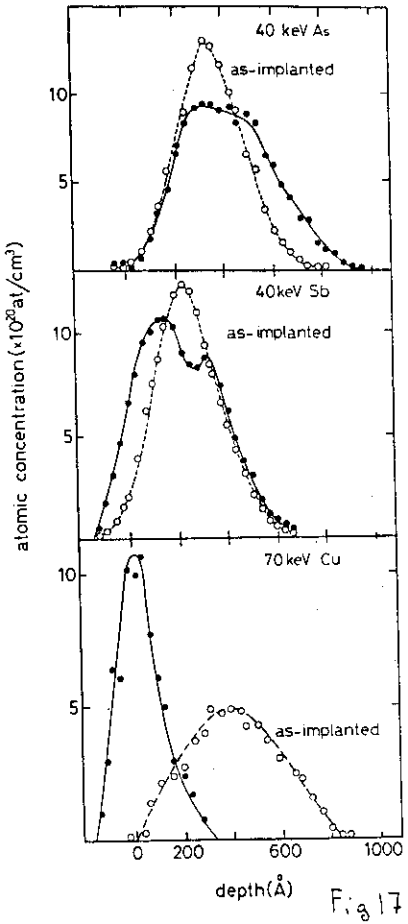

Fig 17

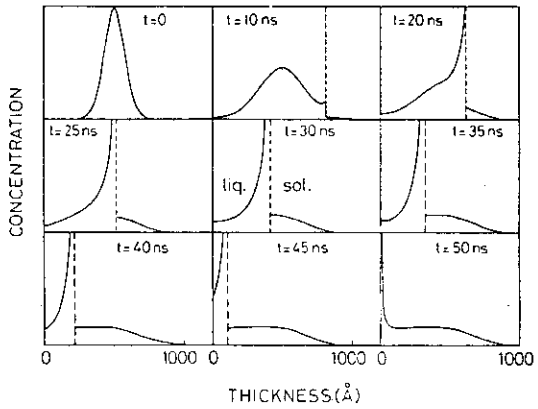

Fig. 18

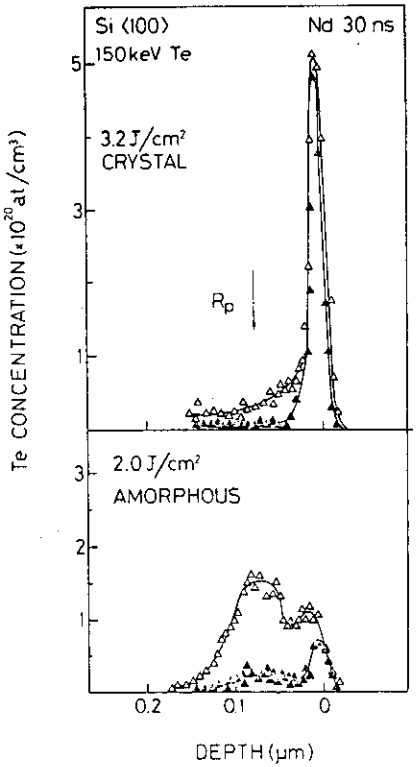

Fig. 20

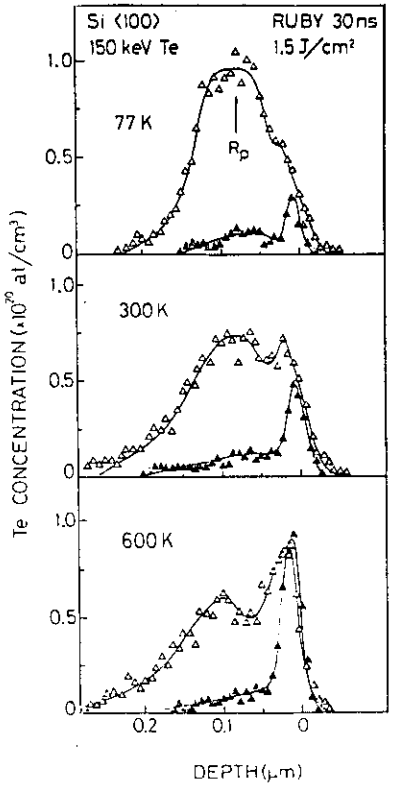

Fig. 21

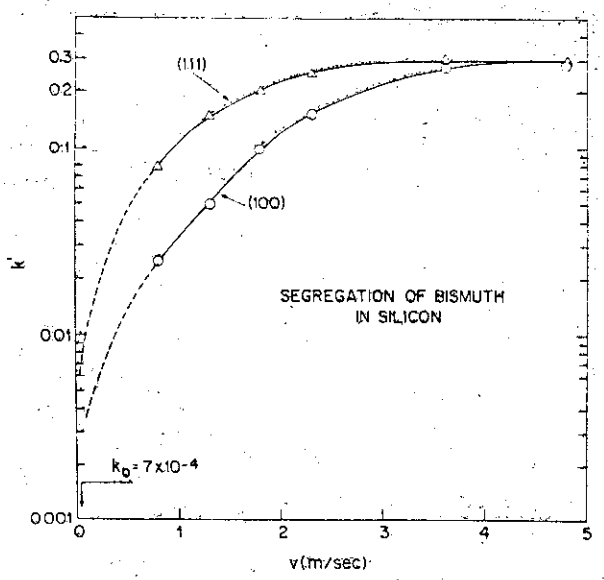
0.3
0.2
0.1
0.01
0.001
k'
(111)
(100)
SEGREGATION OF BISMUTH
IN SILICON
$k_0 = 7 \times 10^{-4}$
0
1
2
3
4
5
v(m/sec)

Fig. 22

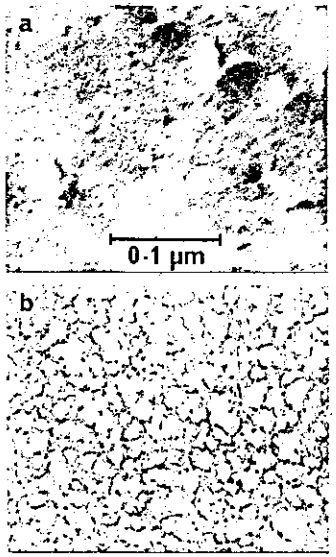
a
0·1 μm
b

Fig. 23